All-optical cw quadruple resonance excitation: A coherently driven five-level molecular system

Ergin H. Ahmed,[*] Peng Qi, and A. Marjatta Lyyra[†]

Department of Physics, Temple University, Philadelphia, Pennsylvania 19122-6082, USA

(Received 13 October 2007; revised manuscript received 19 March 2009; published 18 June 2009)

We report here a continuous-wave, high-resolution, and all-optical quadruple resonance laser excitation experiment. To demonstrate this excitation technique, we have used an inhomogeneously broadened molecular sample (Na_2). We emphasize the enhanced ability afforded by the technique to reach new ranges of internuclear separation as well as access to a large range of molecular electronic states. Using the Autler-Townes split line shape of a rovibronic transition and the E field amplitude of the corresponding coupling laser, we have measured with high precision the absolute value of the molecular electronic transition dipole moment matrix elements, with more flexibility than the double and the triple resonance based excitation schemes used previously. This technique may also be used in a stimulated Raman adiabatic passage configuration for effective transfer of ultracold molecules, formed at long internuclear distance, to the lowest vibrational level of the ground electronic state.

I. INTRODUCTION

Modern spectroscopic techniques based on double and triple resonance excitations have made it possible to study molecular energy levels with unprecedented accuracy, allowing the characterization of molecular potentials for most of the well depth, including coupled systems of singlet and triplet states [1–5]. Nevertheless, some interesting regions of molecular electronic states have been difficult to reach even with triple resonance spectroscopy such as long-range outer wells [6]. In general, studies of vibrational levels with large amplitude vibration in highly excited electronic states have been difficult when starting from the thermally populated ground-state levels due to the exceedingly small overlap integrals in accordance with the Franck-Condon principle [7]. Most of the amplitude of the excited state rovibronic wave function is at the outer turning point of vibration at large internuclear distance, while the wave function amplitude for the thermally populated ground-state levels is mostly confined to the region of the equilibrium internuclear separation. Further, selection rules and limited availability of narrowband tunable laser wavelengths impose additional limits to access to the excited states.

In addition to probing energy-level structure, high-resolution multiple resonance techniques have also made it possible to develop applications of quantum optics for molecular systems, in which many parameters are internuclear distance (R) dependent. For example, by using the Autler-Townes (AT) effect, it has been possible to measure with high accuracy the absolute magnitude of the electronic transition dipole moment matrix element [8–13], a parameter of fundamental importance for the interaction of light with molecular systems. Traditionally, lifetime and intensity measurements were used to determine transition dipole moments [14]. Since molecular excited states can decay to more than

one lower-lying electronic state, lifetime measurements in general probe a combination of several electronic transition moments simultaneously. Calibrated intensity measurements, in turn, yield only a relative value for the transition dipole moment [15]. However, by normalizing the relative calibrated intensity measurements with the Autler-Townes splitting based absolute measurements, as shown in Ref. [12], much weaker transitions can be included and the transition dipole moment function can be characterized over a larger range of internuclear distance.

We report here an all-optical quadruple resonance (AOQR) spectroscopy, which further expands access to electronic states and electronic transition dipole moments beyond the range accessible by double and triple resonance techniques both in terms of electronic and vibrational energies as well as internuclear distance. The initial state can be chosen from within the thermal population of the molecular ground state or from the cold atomic ensemble at the atomic limit. This reversibility aspect is of significant importance for transferring cold molecules [16–22], formed at large internuclear distance by Feshbach resonance or by photoassociation, to the $v''=0$ vibrational state of the molecular ground state using the stimulated Raman adiabatic passage (STIRAP) technique [23–26].

II. EXPERIMENT

The experimental arrangement was nearly the same as described in a previous triple resonance experiment [10]. Sodium vapor was generated in a five-arm heat pipe oven. The temperature of the vapor was estimated to be 550 K from the Doppler line width of a single laser excitation spectrum. Argon was used as a buffer gas with pressure of about 100–200 mTorr. The buffer gas pressure was measured at room temperature. In the experiments three Coherent Autoscan 699-29 dye lasers and a Coherent 899-29 Ti:sapphire laser, all with 0.5 MHz frequency bandwidth, were used. The laser beams were linearly polarized in the same direction. The lasers driving the first two excitations were in a copropagating arrangement, while the third and fourth lasers counterpropagated

---

*Corresponding author. erahmed@temple.edu

†Also at Department of Physics, Lund University, P.O. Box 118, 22100 Lund, Sweden.

relative to them. A mechanical chopper was used to modulate one of the beams for phase-sensitive detection. A SPEX 1404 double grating monochromator was used as a narrow-band filter to detect the molecular fluorescence of a selected single rovibronic fluorescence transition (single channel) in a direction perpendicular to the laser propagation direction.

The spectra were obtained by recording the output of the SPEX photomultiplier tube (Hamamatsu R928) as a function of the probe laser frequency with the computer controlling the probe laser scan. The photomultiplier tube signal was amplified using a lock-in amplifier (SR 850). A combination of a $\lambda/2$ plate and a polarizing prism was used to control the power of the coupling laser, and a neutral density filter was used for the same purpose for the other lasers. Initially the four laser beams were carefully overlapped by maximizing the optical-optical double resonance fluorescence signals of the various two laser combinations. After that, for a finer adjustment of the overlap, we have maximized the magnitude of the detected fluorescence involving all four lasers as well as the magnitude of the observed AT splitting. Once the best possible overlap was achieved, it was kept unchanged during the full length of the particular set of experiments. In order to ensure E field homogeneity of the coupling field in the interaction region in the experiments involving AT splitting, the spot size of the coupling laser was kept about twice as large as the probe and pump laser spot sizes. Tighter focusing of the pump and probe lasers restricted the observed fluorescence to the center of the radial distribution of the coupling laser electric field, and thus the molecules in the overlap region experienced a more uniform coupling laser electric field, leading to a better resolved AT split line profile. The spot size of each of the laser beams w_i, defined as a radius, measured at the $1/e^2$ point of the Gaussian beam profile

$$E_i(r) = E_{i,r=0} \exp\left(-\frac{r^2}{w_i^2}\right)$$

was measured with the razor blade technique [27] in the interaction region. We have estimated by repeated measurements that the error of our spot size measurement is about 10 μm, which is also the smallest step size of the micrometer we used to drive the razor blade across the beam profile. The power of the laser beams was measured with a Coherent Lasermate/D power meter.

The two AOQR excitation schemes used in the experiments are shown in Fig. 1. The population of a rovibrational level $|1\rangle$ of the ground $X\,^1\Sigma_g^+$ state was excited to level $|3\rangle$ through the intermediate level $|2\rangle$ in a two-step excitation with lasers L_1 (Coherent 699-29 laser with R6G 590 dye) and L_2 (Coherent 699-29 laser with DCM dye). The intermediate level $|2\rangle$ was from the $A\,^1\Sigma_u^+$ state, while level $|3\rangle$ was from the $2\,^1\Pi_g$ state. Level $|4\rangle$, again from the $A\,^1\Sigma_u^+$ state, was populated by stimulated emission using laser L_3 (Coherent 699-29 with DCM dye). Levels $|2\rangle$–$|4\rangle$ were used to facilitate the transfer of population to larger internuclear distance by each excitation step. The choice of the specific levels was based on the magnitude of the vibrational overlap integral of the corresponding transitions. Level $|5\rangle$ was
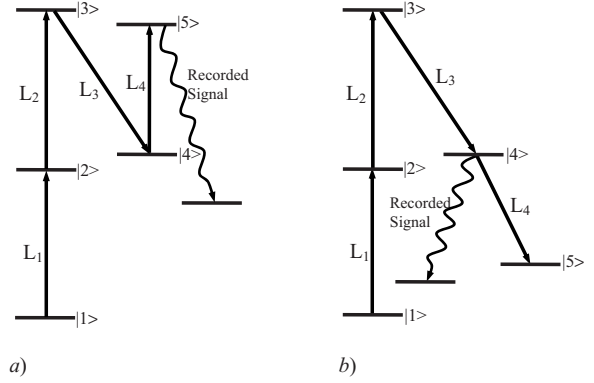
FIG. 1. Energy level diagrams for the two excitation schemes considered. (a) emphasizes transitions between two excited states and (b) emphasizes those between excited and the ground states. Levels $|1\rangle$–$|4\rangle$ are the same for both schemes. Level $|5\rangle$ for (a) belongs to the 4 $^1\Sigma_g^+$ state and to the $X\,^1\Sigma_g^+$ ground state for (b).

coupled to the system by the fourth laser L_4 (Coherent 899-29 Ti:sapphire laser with midwavelength optics). In the excitation scheme labeled (a), level $|5\rangle$ belongs to the excited 4 $^1\Sigma_g^+$ state, while in (b) it is a high-lying level of the ground $X\,^1\Sigma_g^+$ electronic state. In the excitation scheme (a) the signal is detected as single channel fluorescence from the final level $|5\rangle$ or $|4\rangle$, while in scheme (b), with level $|5\rangle$ in the ground state, we have used only single channel fluorescence from level $|4\rangle$. In the experiments involving the Autler-Townes effect L_4 is the coupling laser. The Autler-Townes splitting caused by L_4 is observed in the fluorescence spectra by scanning the frequency of the probe laser L_3 over the $|3\rangle \rightarrow |4\rangle$ resonance, while all other lasers are kept on resonance. The lasers were tuned to the following specific rovibrational transitions: L_1 (16 874.31 cm^{-1}) to $A\,^1\Sigma_u^+(v'=22,\ J'=20)$ $\leftarrow X\,^1\Sigma_g^+(v''=1,\ J''=21)$, L_2 (15 304.86 cm^{-1}) to $2\,^1\Pi_g(v=19,\ J=20) \leftarrow A\,^1\Sigma_u^+(v'=22,\ J'=20)$, L_3 (15 203.84 cm^{-1}) to $2\,^1\Pi_g(v=19,\ J=20) \rightarrow A\,^1\Sigma_u^+(v_1'=23,\ J_1'=20)$, and L_4 (12 545.26 cm^{-1}) to 4 $^1\Sigma_g^+(v_1=14,\ J_1=21)$ $\leftarrow A\,^1\Sigma_u^+(v_1'=23,\ J_1'=20)$ for excitation scheme (a) and (12 533.95 cm^{-1}) to $A\,^1\Sigma_u^+(v_1'=23,\ J_1'=20) \rightarrow X\,^1\Sigma_g^+(v_1''=36,\ J_1''=19)$ for excitation scheme (b).

III. THEORETICAL MODEL

To simulate theoretically our experimental results we have followed standard density-matrix formalism [28,29]. The evolution of the density matrix $\rho(\mathbf{v},\mathbf{r},t)$ of our system in time and space is governed by the equation of motion

$$\frac{\partial\rho}{\partial t} = -\frac{i}{\hbar}[H,\rho] + \Gamma(\rho). \qquad (1)$$

In the interaction picture, the Hamiltonian H for the system, depicted in Fig. 1, has the form

$$H = \hbar\sum_{i=1}^{4}\sum_{j=1}^{i}\delta_j|i+1\rangle\langle i+1| + \frac{\hbar}{2}\sum_{i=1}^{4}\Omega_i(|i+1\rangle\langle i| + |i\rangle\langle i+1|), \qquad (2)$$

We define the velocity-dependent detuning of the lasers from the molecular transitions by $\delta_j \equiv \mathrm{sign}(\varepsilon_{j+1}-\varepsilon_j)\Delta_j \pm k_j v_z$,

where $\text{sign}(\varepsilon_{j+1}-\varepsilon_j)$ is the sign of the energy difference of levels $|j+1\rangle$ and $|j\rangle$ connected by the jth laser and the sign for $\pm k_j v_z$ is chosen in accordance with the jth laser propagation direction. Here k_i is the wave number of the corresponding laser and v_z is the molecular velocity along the laser propagation direction. The laser detuning from resonance is $\Delta_i = \omega_{i+1,i} - \omega_i$. With $\omega_{i+1,i}$ we denote the molecular transition frequency between the levels $|i+1\rangle$ and $|i\rangle$, with ω_i as the frequency of the ith laser (L_i). The Rabi frequency Ω_i of the ith laser is defined by $\Omega_i \equiv \frac{\mu_{i,i+1}E_i}{\hbar}$, where $\mu_{i,i+1} = \langle \psi_{v_{i+1}j_{i+1}} | \mu_e(R) | \psi_{v_j j_i} \rangle$ is the total transition dipole moment matrix element and $\mu_e(R)$ denotes the electronic component of the transition dipole moment as a function of internuclear distance R.

Every molecular level can decay to lower-lying electronic states of the system through spontaneous emission, as well as through other processes such as collisions, etc. These are incorporated in the density-matrix equation of motion by means of an $n \times n$ relaxation matrix $\Gamma(\rho)$. The elements of the matrix $\Gamma(\rho)$ in general can be presented in the form

$$\Gamma_{ij}(\rho) = \delta_{ij}\left(-W_i \rho_{ij} + \sum_{\substack{k=1 \\ k \neq i}}^{n} \Theta(\varepsilon_k - \varepsilon_i)(W_{ki} + W_t)\rho_{kk}\right) - (1 - \delta_{ij})\gamma_{ij}\rho_{ij},$$ (3)

where δ_{ij} is the Kronecker delta and $\Theta(\varepsilon_k - \varepsilon_i)$ is the Heaviside step function. With W_{ij} we denote the radiative decay rate from level i to j, W_i is the total radiative decay rate of level i ($W_i = 1/\tau_i$, where τ_i is the radiative lifetime of the state i) and γ_{ij} are the phenomenological parameters representing the damping rate, at which the off-diagonal elements of the density matrix relax toward equilibrium, defined by

$$\gamma_{nm} = \frac{1}{2}\sum_k (W_{nk} + W_{mk}) + \gamma_{nm}^c, \quad n \neq m.$$ (4)

The γ_{nm}^c parameters represent the dependence of the decay processes on collisions with other atoms or molecules. For levels that cannot decay radiatively, as is the case of level $|5\rangle$ in the excitation scheme of Fig. 1(b), the rate with which the molecules escape the interaction region (beam transit rate W_t) is the dominant process and has be taken into account. For our system W_t is on the order of 1 MHz, calculated according to Ref. [30].

The Na_2 molecular system can be considered as open in the sense that the energy levels used to create the coherence effect are also coupled to other energy levels outside the excitation scheme. Therefore, the total population of the five coherently coupled levels $|1\rangle$–$|5\rangle$ of an open system is strongly not conserved, due to the many extra rovibrational decay pathways for the excited levels as shown in Fig. 2. This is in contrast to a closed atomic system, in which no other levels beyond those needed to create the coherence effect are involved. In order to take into account this "openness" of the coherently coupled levels, we introduce two auxiliary states denoted by $|6\rangle$ and $|7\rangle$, which represent all other rovibrational states of the A and the X manifolds, respectively, to which decays are possible. All simulations in-
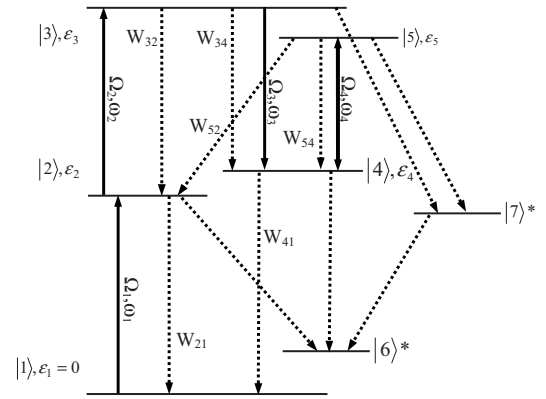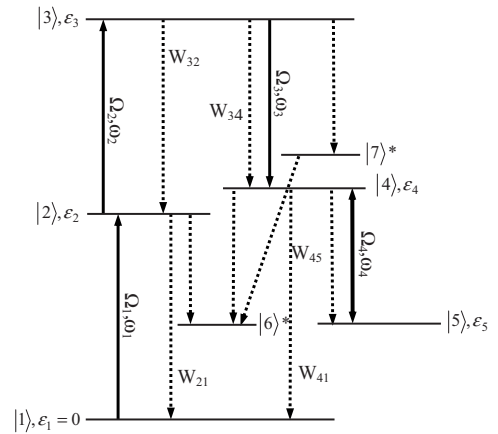
FIG. 2. Schematics of the excitation and decay processes of the two five-level quadruple resonance experiments. Due to selection rules W_{31}, W_{35}, and W_{37} are zero in the particular case of Na_2. The energy levels $|1\rangle$–$|5\rangle$ correspond to the rovibronic energy levels of Fig. 1. The solid arrows indicate the lasers with the Rabi and photon frequencies specified. The dashed arrows indicate the decay channels. Levels $|6\rangle^*$ and $|7\rangle^*$ represent all other rovibrational states of the X and A manifolds to which decay is possible.

cluded averaging over the molecular velocity distribution, summation over the magnetic sublevels M_J, and averaging over the radial distribution of the laser fields. After calculating the density-matrix elements and performing all the required averaging, the population of level $|5\rangle$ in the excitation scheme (a), and level $|4\rangle$ in system (b), represented by $\langle\rho_{55}\rangle$ and $\langle\rho_{44}\rangle$ up to a constant of proportionality, is interpreted as the fluorescence signal of a specific decay path (single channel) from these levels as a function of the detuning of the probe laser.

IV. RESULTS AND DISCUSSION

Using the excitation scheme of Fig. 1(a) we have investigated the enhancement in the population of the final target state $|5\rangle$ due to stimulated emission between levels $|3\rangle$ and $|4\rangle$ in comparison to the case when there is only population transfer due to fluorescence. This demonstrates the advantage of quadruple resonance excitation compared to the fluorescence enhanced triple resonance excitation scheme. Figure 3 shows that there is a significant enhancement in the popula-
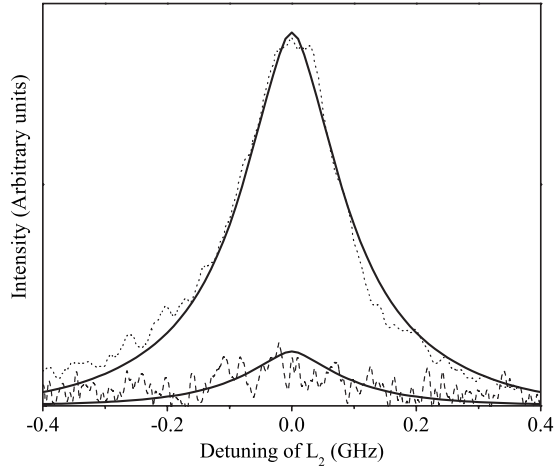
FIG. 3. Quadruple resonance single channel fluorescence spectra from level $|5\rangle$ using the scheme of Fig. 1(a). The dashed line represents the fluorescence enhanced triple resonance case (laser L_3 was blocked). In this case the transition between levels $|3\rangle$ and $|4\rangle$ is only due to spontaneous emission. The dotted line represents the quadruple resonance case, where the transition from $|3\rangle$ to $|4\rangle$ is coherently driven by L_3. Our theoretical simulations are shown with a solid line. The Rabi frequencies at the center of the laser beams are 56, 104, 228, and 275 MHz for L_1–L_4, correspondingly. The laser beam spot sizes w_i (defined as radius) are 300, 280, 405, and 660 μm for L_1–L_4, correspondingly.

tion of level $|5\rangle$, when the transition $|3\rangle$–$|4\rangle$ is coherently driven (dotted line, quadruple resonance), in comparison with the case when the population transfer from level $|3\rangle$ to $|4\rangle$ is only due to spontaneous emission (dashed line, triple resonance). The spectra in Fig. 3 are obtained by recording the fluorescence from level $|5\rangle$ using a monochromator positioned at 685.79 nm for the $4\,^1\Sigma_g^+(14,21)$-$A\,^1\Sigma_u^+(4,20)$ transition as a function of the detuning of L_2. The enhancement of the population in the final state is on the order of a factor of 6. The simulations of the experimental results are performed with the density-matrix model described above using as parameters the Rabi frequencies of the lasers calculated [10] from the experimentally measured laser powers and the transition dipole moment matrix elements given in Table I. The lifetime of the $A\,^1\Sigma_u^+$ levels $|2\rangle$ and $|4\rangle$: $\tau=12.5$ ns [31]; the lifetime of the $2\,^1\Pi_g$ level $|3\rangle$: $\tau=18.3$ ns; the lifetime of the $4\,^1\Sigma_u^+$ state: $\tau=12.2$ ns; the branching ratios W_{ij}/W_i calculated from the Franck-Condon factors (see Table I) of the

corresponding transitions; temperature of 550 K. The lifetimes of the rovibrational levels from the $2\,^1\Pi_g$ and the $4\,^1\Sigma_u^+$ states were calculated using the general procedure outlined in [32] with the computer program LEVEL [33] and the potential curves of the relevant electronic states [4,34–36]. In addition to representing well the general shape of the spectra, the model correctly accounts for the relative intensity difference between the two spectra due to the presence or the absence of laser L_3.

Using the Autler-Townes effect associated with the AOQR technique, the transition dipole moment between a variety of molecular electronic states can also be measured very accurately. This was demonstrated for double and triple resonance excitation in Refs. [9,10]. To demonstrate the versatility of the quadruple resonance technique compared to the previous experiments, we have measured the transition dipole moment between specific rovibrational levels of the $4\,^1\Sigma_g^+$ and the $A\,^1\Sigma_u^+$ electronic states, using the excitation scheme of Fig. 1(a), as well as between the $A\,^1\Sigma_u^+$ and the $X\,^1\Sigma_g^+$ electronic states using the excitation scheme of Fig. 1(b). For the first case the spot sizes of the lasers w in the experiments were 360, 285, 450, and 480 μm for L_1 to L_4 and for the latter 300, 405, 278, and 505 μm for L_1 to L_4, respectively. In order to minimize the influence of the pump lasers L_1 and L_2 and the probe laser L_3 on the observed Autler-Townes splitting, their power levels were kept as low as possible, while still maintaining a good signal to noise ratio in the recorded spectra. To minimize the effect of pump and probe lasers on the observed AT splitting in the spectrum, their power was kept as low as possible, while still maintaining good signal to noise ratio. We found that the laser power combination of $\sim$60, $\sim$100, and $\sim$35 mW for L_1, L_2, and L_3, respectively, with the given laser beam spot sizes was optimal. Furthermore, the power of the coupling laser L_4 was changed between 100 and 700 mW by using a combination of a polarizing beam splitter cube and a half-wave-plate, while the power of the other three lasers was kept at the desired constant values using neutral density filters. The reason for this was to avoid distortion of the coupling laser Gaussian beam profile by the neutral density filters with the higher coupling laser power levels. The experiments indicate, as expected and demonstrated in Fig. 4, a linear dependence between the observed Autler-Townes splitting and the coupling field Rabi frequency. During each experiment the AT split fluorescence signal was recorded as a function of the probe laser (L_3) detuning while the pump

TABLE I. The Franck-Condon factors ($|\langle v'J'|v''J''\rangle|^2$) and the transition dipole moment matrix elements $[\mu=|\langle v'J'|\mu_e(R)|v''J''\rangle|]$ listed are calculated from *ab initio* electronic transition dipole moment functions $\mu_e(R)$ [10,38] and the potential curves of the electronic states [4,34,35,45,46] using the computer program LEVEL [33].

Transition	Franck-Condon factors	μ (D)
$A\,^1\Sigma_u^+(v'=22,\ J'=20) \leftarrow X\,^1\Sigma_g^+(v=1,\ J=21)$	0.008	0.78
$2\,^1\Pi_g(v=19,\ J=20) \leftarrow A\,^1\Sigma_u^+(v'=22,\ J'=20)$	0.050	1.40
$2\,^1\Pi_g(v=19,\ J=20) \rightarrow A\,^1\Sigma_u^+(v_1'=23,\ J_1'=20)$	0.168	2.66
$4\,^1\Sigma_g^+(v_1=14,\ J_1=21) \leftarrow A\,^1\Sigma_u^+(v_1'=23,\ J_1'=20)$	0.190	3.11
$A\,^1\Sigma_u^+(v_1'=23,\ J_1'=20) \rightarrow X\,^1\Sigma_g^+(v_1''=36,\ J_1''=19)$	0.232	5.05
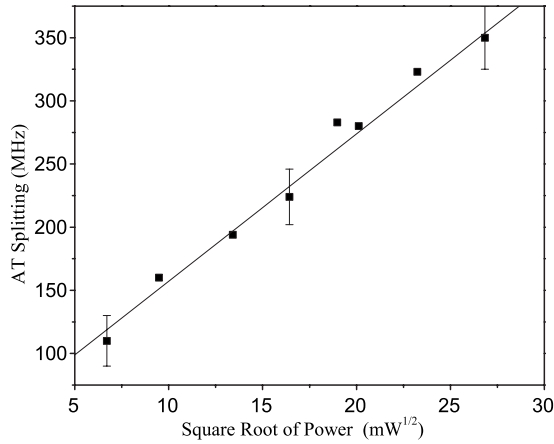
FIG. 4. The Autler-Townes splitting observed in the fluorescence spectrum from level $|4\rangle$ using excitation scheme of Fig. 1(b) versus the square root of the total coupling power P for the $A\ ^1\Sigma_u^+(23,20) \rightarrow X\ ^1\Sigma_g^+(36,19)$ transition. The experimentally measured AT splitting is shown by solid squares, while the solid line is a linear fit for these points.

lasers (L_1 and L_2) and the coupling laser (L_4) were kept on resonance. Sample AT split spectra for the two excitation schemes are shown in Fig. 5, where the spectra were recorded by monitoring the fluorescence of a specific rovibrational transition from level $|4\rangle$, $A\ ^1\Sigma_u^+(v'=23,\ J'=20) \rightarrow X\ ^1\Sigma_g^+(v''=3,\ J''=21)$, as a function of the detuning of the probe laser.

The simulations of the recorded spectra were performed in a similar way to the ones in Fig. 3. The only difference is that the Rabi frequency of the coupling field Ω_4 was varied until the best fit to the recorded experimental spectrum was obtained. The transition dipole moment matrix element between the rovibrational levels coupled by L_4 was calculated from the value of Ω_4 determined in this manner and from the amplitude of the coupling laser electric field E_4. We note that the peak to peak separation of the well-resolved Autler-Townes split line shape is insensitive to the lifetimes of the energy levels. We have obtained $\mu_{exp}=4.87$ D and $\mu_{exp}=3.2$ D for the transition dipole moments of $A\ ^1\Sigma_u^+(23,20)$-$X\ ^1\Sigma_g^+(36,19)$ and $4\ ^1\Sigma_g^+(14,19)$-$X\ ^1\Sigma_g^+(23,20)$ transitions, respectively. The values compare well with the values obtained using an *ab initio* calculated electronic transition dipole moment function $\mu_e(R)$ [10,37] of 5.05 and 3.1 D [38] for the $A\ ^1\Sigma_u^+(23,20)$-$X\ ^1\Sigma_g^+(36,19)$ and the $4\ ^1\Sigma_g^+(14,19)$-$X\ ^1\Sigma_g^+(23,20)$ systems, respectively. The main error in the transition dipole moment determination in our case arises from experimental error in the measurement of the electric field amplitude E_4 of the coupling laser. We estimate conservatively that for a typical 500 mW coupling laser focused to a spot size of 450 to $550 \pm 10\ \mu$m, the relative error in the electric field measurement is about 4%. The transition dipole moment measurements between the ground and the excited states [10] as well as between two excited states [9] can be performed using the simpler double and triple resonance excitation schemes [2,10]. However, a major drawback of these two schemes is that the pump and the coupling lasers share a common level. This imposes a

(a)

(b)
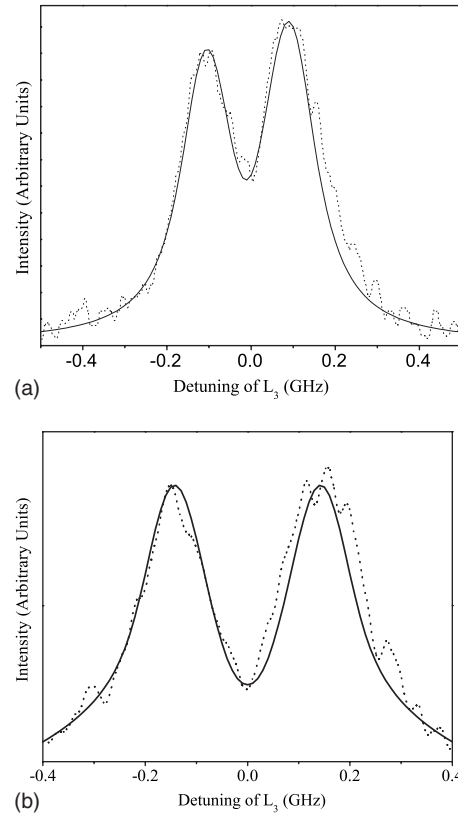
FIG. 5. The dotted lines show sample experimental fluorescence AT split spectra obtained using the excitation schemes from Figs. 1(a) and 1(b), respectively. The spectra were recorded while L_1, L_2, and L_4 were held fixed on resonance and the probe laser L_3 was modulated and scanned. The coupling field laser powers were 585 mW for (a) and 405 mW for (b). The solid line is the result of a simulation using the density-matrix formalism with coupling Rabi frequency $\Omega_4=560$ MHz and detuning $\Delta_4=15$ MHz for spectrum (a) and $\Omega_4=940$ MHz and $\Delta_4=0$ for spectrum (b).

severe limitation on the choice of the coupling transition due to the requirement that the pump transition has at least a modest Franck-Condon factor and that it starts from a thermally populated rovibrational level of the ground electronic state. In contrast, using the AOQR scheme, the presence of a number of excitation steps leading from the thermally populated ground state $|1\rangle$ to level $|4\rangle$ facilitates access to a very large set of coupling transition ($|4\rangle \leftrightarrow |5\rangle$). In this manner the AOQR technique, with the Autler-Townes effect incorporated, enhances the possibility for obtaining the electronic transition dipole moment $\mu_e(R)$ between the ground and the excited states [11,13] as well as between two excited states [12] as a function of the internuclear distance R using the concept of the R-centroid approximation [39–42] for rovibronic transitions. Mapping the internuclear distance dependence of the electronic transition dipole moment $\mu_e(R)$ is of fundamental importance because it is at the heart of the interaction of light with molecules and provides a critical test of *ab initio* calculated transition dipole moment functions [10,13,43,44]. Accurate molecular oscillator strengths are also critical in many applications.
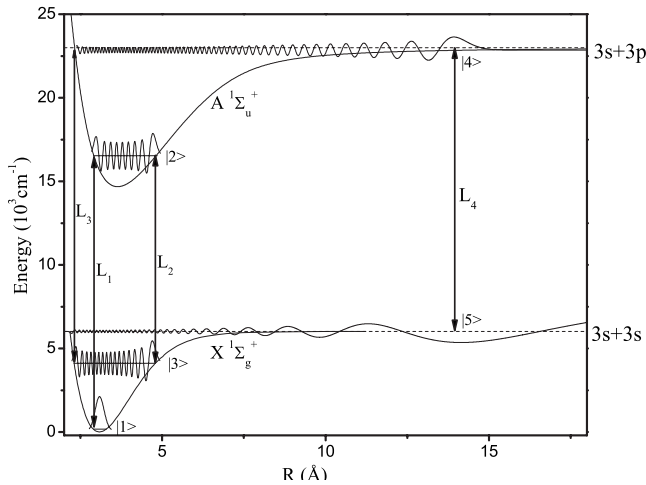
FIG. 6. Schematic of a quadruple resonance experiment that can be used in combination with chainwise STIRAP technique for population transfer of ultracold Na_2 formed at large internuclear distance R to the ground-state vibrational level $v''=0$. The levels labeled $|1\rangle-|5\rangle$ are $X\,^1\Sigma_g^+(v''=0,\ J''=0)$, $A\,^1\Sigma_u^+(v'=16,\ J'=1)$, $X\,^1\Sigma_g^+(v_1''=30,\ J_1''=0)$, $A\,^1\Sigma_u^+(v_1'=120,\ J_1'=1)$, and $X\,^1\Sigma_g^+(v_2''=65,\ J_2''=0)$, respectively.

V. CONCLUSION

We have performed a cw all-optical quadruple resonance excitation experiment with all excitation steps being coher-ently driven by a combination of four tunable cw lasers. This excitation technique is very general and can be used to probe transitions to electronic states over a wide range of internu-clear distance. It is also advantageously applicable to atomic systems since they have much stronger transitions. The Autler-Townes effect associated with this technique can be used to investigate the internuclear distance dependence of the transition dipole moment function. By choosing different coupling laser transitions corresponding to different R-centroid values, this technique extends the range of acces-sible internuclear distance in different electronic states con-siderably both for measuring energy-level positions as well as the value of the transition dipole moment matrix element. We believe that the AOQR technique can also be used in the STIRAP configuration to create cold molecular samples in their ground vibrational state from cold molecules formed at long range [17]. Figure 6 illustrates a possible excitation scheme for such an application. It may also be possible to reach Rydberg states with large amplitude vibration using this excitation scheme [47].

[1] R. W. Field, M. Revelli, and G. A. Capelle, J. Chem. Phys. **63**, 3228 (1975).

[2] A. M. Lyyra, H. Wang, T.-J. Whang, W. C. Stwalley, and L. Li, Phys. Rev. Lett. **66**, 2724 (1991).

[3] K. M. Jones, E. Tiesinga, P. D. Lett, and P. S. Julienne, Rev. Mod. Phys. **78**, 483 (2006).

[4] P. Qi, J. Bai, E. Ahmed, A. M. Lyyra, S. Kotochigova, A. J. Ross, C. Effantin, P. Zalicki, J. Vigué, G. Chawla, R. W. Field, T.-J. Whang, W. C. Stwalley, H. Knöckel, E. Tiemann, J. Shang, L. Li, and T. Bergeman, J. Chem. Phys. **127**, 044301 (2007).

[5] M. R. Manaa, A. J. Ross, F. Martin, P. Crozet, A. M. Lyyra, L. Li, C. Amiot, and T. Bergeman, J. Chem. Phys. **117**, 11208 (2002).

[6] C.-C. Tsai, J. T. Bahns, and W. C. Stwalley, J. Chem. Phys. **99**, 7417 (1993).

[7] E. U. Condon, Phys. Rev. **32**, 858 (1928).

[8] J. Qi, G. Lazarov, X. Wang, L. Li, L. M. Narducci, A. M. Lyyra, and F. C. Spano, Phys. Rev. Lett. **83**, 288 (1999).

[9] J. Qi, F. C. Spano, T. Kirova, A. Lazoudis, J. Magnes, L. Li, L. M. Narducci, R. W. Field, and A. M. Lyyra, Phys. Rev. Lett. **88**, 173003 (2002).

[10] E. Ahmed, A. Hansson, P. Qi, T. Kirova, A. Lazoudis, S. Ko-tochigova, A. M. Lyyra, L. Li, J. Qi, and S. Magnier, J. Chem. Phys. **124**, 084308 (2006).

[11] E. H. Ahmed, P. Qi, B. Beser, J. Bai, R. W. Field, J. P. Huen-nekens, and A. M. Lyyra, Phys. Rev. A **77**, 053414 (2008).

[12] S. J. Sweeney, E. H. Ahmed, P. Qi, T. Kirova, A. M. Lyyra, and J. Huennekens, J. Chem. Phys. **129**, 154303 (2008).

[13] O. Salihoglu, P. Qi, E. H. Ahmed, S. Kotochigova, S. Magnier, and A. M. Lyyra, J. Chem. Phys. **129**, 174301 (2008).

[14] A. C. G. Mitchell and M. W. Zemansky, *Resonance Radiation and Excited Atoms* (Cambridge University Press, Cambridge, England, 1971).

[15] E. Laub, I. Mazsa, S. C. Webb, J. L. Civita, I. Prodan, Z. J. Jabbour, R. K. Namiotka, and J. Huennekens, J. Mol. Spec-trosc. **193**, 376 (1999); **221**, 142(E) (2003).

[16] M. J. Mark, J. G. Danzl, E. Haller, M. Gustavsson, N. Boulo-ufa, O. Dulieu, H. Salami, T. Bergeman, H. Ritsch, R. Hart, and H.-C. Nägerl, Appl. Phys. B: Lasers Opt. **95**, 219 (2009).

[17] E. Kuznetsova, P. Pellegrini, R. Cote, M. D. Lukin, and S. F. Yelin, Phys. Rev. A **78**, 021402(R) (2008).

[18] W. C. Stwalley, Eur. Phys. J. D **31**, 221 (2004).

[19] K. Winkler, F. Lang, G. Thalhammer, P. v. d. Straten, R. Grimm, and J. H. Denschlag, Phys. Rev. Lett. **98**, 043201 (2007).

[20] J. G. Danzl, E. Haller, M. Gustavsson, M. J. Mark, R. Hart, N. Bouloufa, O. Dulieu, H. Ritsch, and H. C. Nagerl, Science **321**, 1062 (2008).

[21] K. K. Ni, S. Ospelkaus, M. H. G. de Miranda, A. Pe'er, B. Neyenhuis, J. J. Zirbel, S. Kotochigova, P. S. Julienne, D. S. Jin, and J. Ye, Science **322**, 231 (2008).

[22] F. Lang, K. Winkler, C. Strauss, R. Grimm, and J. Hecker Denschlag, Phys. Rev. Lett. **101**, 133005 (2008).

[23] J. Oreg, F. T. Hioe, and J. H. Eberly, Phys. Rev. A **29**, 690 (1984).

[24] J. R. Kuklinski, U. Gaubatz, F. T. Hioe, and K. Bergmann, Phys. Rev. A **40**, 6741 (1989).

[25] S. Schiemann, A. Kuhn, S. Steuerwald, and K. Bergmann, Phys. Rev. Lett. **71**, 3637 (1993).

[26] K. Bergmann, H. Theuer, and B. W. Shore, Rev. Mod. Phys. **70**, 1003 (1998).

[27] D. R. Skinner and R. E. Whitcher, J. Phys. E **5**, 237 (1972).

[28] S. Stenholm, *Foundations of Laser Spectroscopy* (Wiley Interscience, New York, 1984).

[29] M. O. Scully and M. S. Zubairy, *Quantum Optics* (Cambridge University Press, Cambridge, England, 2002).

[30] J. Sagle, R. K. Namiotka, and J. Huennekens, J. Phys. B **29**, 2629 (1996).

[31] G. Baumgartner, H. Kornmeier, and W. Preuss, Chem. Phys. Lett. **107**, 13 (1984).

[32] A. Hansson and J. G. Watson, J. Mol. Spectrosc. **233**, 169 (2005).

[33] R. J. Le Roy, University of Waterloo Chemical Physics Research Report No. CP663, 2007 (unpublished).

[34] T.-J. Whang, H. Wang, A. M. Lyyra, L. Li, and W. C. Stwalley, J. Mol. Spectrosc. **145**, 112 (1991).

[35] C.-C. Tsai, J. T. Bahns, H. Wang, T.-J. Wang, and W. C. Stwalley, J. Chem. Phys. **101**, 25 (1994).

[36] H. Richter, H. Knockel, and E. Tiemann, Chem. Phys. **157**, 217 (1991).

[37] S. Kotochigova, E. Tiesinga, and I. Tupitsyn, *New Trends in Quantum Systems in Physics and Chemistry* (Kluwer Academic, Dordrecht, The Netherlands, 2001).

[38] The transition dipole moment functions $\mu_e(R)$ between the electronic states $4\ ^1\Sigma_g^+$-$A\ ^1\Sigma_u^+$ and $2\ ^1\Pi_g$-$A\ ^1\Sigma_u^+$ was provided by S. Magnier (private communication).

[39] P. A. Fraser, Can. J. Phys. **32**, 515 (1954).

[40] J. Tellinghuisen, in *The Franck-Condon Principle in Bound-Free Transitions*, edited by K. P. Lawley, Advances in Chemical Physics Vol. 60 (Wiley, New York, 1985), pp. 299–369.

[41] C. Noda and R. N. Zare, J. Mol. Spectrosc. **95**, 254 (1982).

[42] H. Lefebvre-Brion and R. W. Field, *The Spectra and Dynamics of Diatomic Molecules* (Elsevier, Amsterdam, 2004).

[43] S. Soorkia, F. Le Quere, C. Leonard, and D. Figgen, Mol. Phys. **105**, 1095 (2007).

[44] D. D. Konowalow, M. E. Rosenkrantz, and D. S. Hochhauser, J. Mol. Spectrosc. **99**, 321 (1983).

[45] P. Kusch and M. M. Hessel, J. Chem. Phys. **68**, 2591 (1978).

[46] O. Babaky and K. Hussein, Can. J. Phys. **67**, 9112 (1989).

[47] C. H. Greene, A. S. Dickinson, and H. R. Sadeghpour, Phys. Rev. Lett. **85**, 2458 (2000).